



UNIVERSIDADE ESTADUAL DE CAMPINAS
SISTEMA DE BIBLIOTECAS DA UNICAMP
REPOSITÓRIO DA PRODUÇÃO CIENTÍFICA E INTELLECTUAL DA UNICAMP

Versão do arquivo anexado / Version of attached file:

Versão do Editor / Published Version

Mais informações no site da editora / Further information on publisher's website:

<https://www.sciencedirect.com/science/article/pii/S1751616115003574>

DOI: 10.1016/j.jmbbm.2015.09.020

Direitos autorais / Publisher's copyright statement:

©2016 by Elsevier. All rights reserved.

DIRETORIA DE TRATAMENTO DA INFORMAÇÃO

Cidade Universitária Zeferino Vaz Barão Geraldo

CEP 13083-970 – Campinas SP

Fone: (19) 3521-6493

<http://www.repositorio.unicamp.br>

Available online at www.sciencedirect.com

ScienceDirect

www.elsevier.com/locate/jmbbm

Research paper

Ductility improvement due to martensite α' decomposition in porous Ti–6Al–4V parts produced by selective laser melting for orthopedic implants

E. Sallica-Leva^a, R. Caram^a, A.L. Jardini^b, J.B. Fogagnolo^{a,*}^aUniversity of Campinas, School of Mechanical Engineering, Rua Mendeleiev 200, 13083-860 Campinas, SP, Brazil^bUniversity of Campinas, School of Chemical Engineering, Av. Albert Einstein 500, 13083-852 Campinas, Brazil

ARTICLE INFO

Article history:

Received 23 June 2015

Received in revised form

18 September 2015

Accepted 19 September 2015

Available online 28 September 2015

Keywords:

Titanium alloys

Additive manufacturing

Thermal treatment

Thermal analysis

X-ray analysis

Mechanical properties

ABSTRACT

Ti–6Al–4V parts obtained by selective laser melting typically have an acicular α' martensitic microstructure whose ductility is low. Thus, post-heat treatments are useful for increasing ductility. In this work, the effects of sub- β -transus heat treatments on the mechanical properties of Ti–6Al–4V parts with porous structures are correlated with martensite α' phase decomposition. The precipitation of β phase and the gradual transformation of α' into α phase by the diffusion of excess vanadium from α' to β phase are proposed to be the main events of martensite α' phase decomposition in parts fabricated by selective laser melting. The heat treatment performed at 650 °C for 1 h produced no microstructural changes, but the samples treated for at the same temperature 2 h showed a fine precipitation of β phase along the α' needle boundaries. The heat treatment performed at 800 °C for 1 or 2 h produced a fine α + β microstructure, in which β phase are present as particles fewer in number and larger in size, when compared with the ones present in the sample heat-treated at 650 °C for 2 h. Heat-treatment of the parts at 800 °C for 2 h proved to be the best condition, which improved the ductility of the samples while only slightly reducing their strength.

© 2015 Elsevier Ltd. All rights reserved.

1. Introduction

The fabrication of titanium and titanium alloy parts with porous structures offers an alternative to decrease the stiffness of orthopedic implants and overcome undesirable stress shielding, which is a consequence of the high mismatch between the stiffness of the metallic implant and that of human bone. Furthermore, porous structures have additional

advantages over full-density material: they are lighter and the architecture of interconnected pores enables new tissue to grow through them, improving implant fixation (Warnke et al., 2009).

Additive manufacturing technologies such as selective laser melting (SLM) and electron beam melting (EBM) allow one to produce parts with controlled internal pore structures or fully densified parts of complex geometries. SLM is a technique

*Corresponding author. Tel.: +55 19 35213300; fax: +55 19 3289 3722.

E-mail address: fogagnolo@fem.unicamp.br (J.B. Fogagnolo).

whereby parts are produced from metal powder, using the energy of a laser beam to selectively promote fusion according to a previously defined CAD model. The process occurs inside a thermally controlled chamber with inert gas (Yang et al., 2002; Vandenbroucke and Kruth, 2007).

Ti-6Al-4V alloy, which was initially developed for aerospace applications, is widely used today in orthopedic implants owing to features such as high strength-to-weight ratio, low Young's modulus, high corrosion resistance and good biocompatibility in the physiological environment (Liu et al., 2004; Geetha et al., 2009). This alloy is also the titanium alloy most widely used in additive manufacturing. Ti-6Al-4V parts produced by SLM present high residual stress in the as-processed state and possess a typically acicular α' martensitic microstructure. Hence, their ductility is low, but post-heat treatments can be applied to overcome this disadvantage.

There are numerous studies about the effects of heat treatments on the mechanical properties of Ti-6Al-4V alloy obtained by more conventional processes (Ahmed and Rack, 1998; Venkatesh et al., 2009; Dong et al., 2013), and several points regarding this subject are well established. Annealing temperatures lower than 550 °C should be avoided due to very fine Ti_3Al precipitation, which promotes age hardening and embrittlement (Lütjering, 1998). Annealing temperatures above the β -transus (super- β -transus treatments) should also be avoided, due to excessive grain growth of the β phase in this range of temperatures. Annealing temperatures in the two-phase field (sub- β -transus treatments) can improve the mechanical strength and do not significantly reduce ductility (Fan et al., 2011).

More recently, the effects of heat treatments on the mechanical properties of Ti-6Al-4V parts obtained by SLM were reported by Vrancken et al. (2012). These authors showed that the response of SLM material to heat treatment differs considerably from that of conventionally processed Ti-6Al-4V alloy. One of the main causes for the differences is the condition of the starting material. The alloy produced by more conventional processes is in the annealed or heavily deformed condition, while, as stated earlier, SLM parts characteristically have a martensitic α' microstructure. Therefore, the effect of heating on the martensitic α' phase must be understood in order to

design heat treatments at sub- β -transus temperature, aimed at increasing the material's ductility. In an earlier study, we examined the effect of pore size and volume fraction of porosity on the mechanical properties of Ti-6Al-4V porous parts obtained by SLM (Sallica-Leva et al., 2013). The effect of the cooling rate in super- β -transus treatments was also analyzed. In this work, we studied the effects of sub- β -transus heat treatments on the mechanical properties of Ti-6Al-4V porous structures, emphasizing the role of martensite α' phase decomposition.

2. Experimental details

The porous part was first designed by CAD, using the cubic body with 15 mm edge created by Parthasarathy et al. (2010), which was reproduced and characterized in a previous study (Sallica-Leva et al., 2013). We used the model with 68% of porosity, a pore size of 1570 μm and strut size of 800 μm . The porous parts were then produced by SLM, using a Ti-6Al-4V pre-alloyed powder as raw material. The following process parameters were selected: 170 W laser power, 1250 mm/s scan speed, 100 μm distance between laser scan lines, and 30 μm layer thickness. Fig. 1 depicts the CAD model and a sample fabricated by SLM technique. The non-heat-treated samples that will be used for purposes of comparison are hereinafter referred to as as-processed samples.

The martensitic α' microstructure revealed by Kroll's reagent was observed in as-processed samples, as shown in Fig. 2. This structure resulted from the high cooling rate imposed by the SLM process (Elmer et al., 2004; Murr et al., 2009; Facchini et al., 2010). The nitrogen-oxygen level, which was determined by the inert gas fusion method using a LECO TC400 nitrogen-oxygen analyzer, was found to be $0.021 \pm 0.003\%$ and $0.170 \pm 0.004\%$, respectively, in the as-processed samples. The as-processed samples exhibited an effective elastic modulus (E_{eff}) of 7.72 ± 0.04 GPa, yield strength (YS) of 129 ± 4 MPa, ultimate compressive strength (UCS) of 163 ± 2 MPa, hardness of 277 ± 9 HV and fracture strain of $8.23 \pm 0.40\%$. Further details about porous parts fabrication and characterization can be found in an earlier paper (Sallica-Leva et al., 2013).

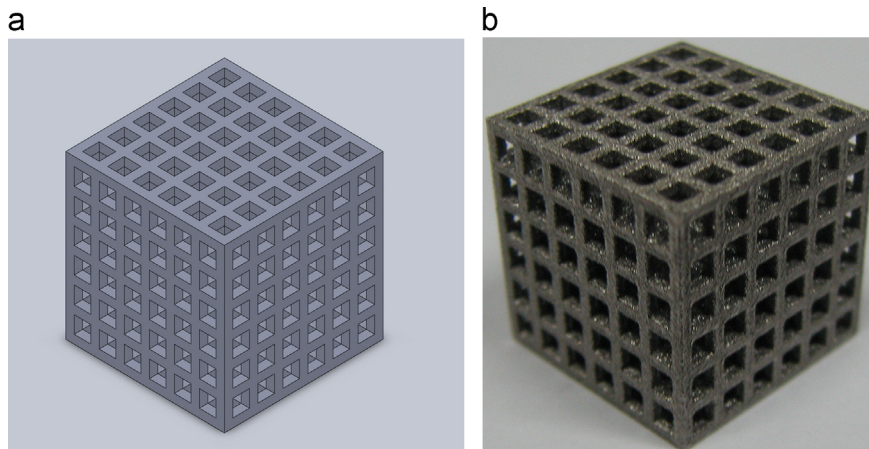


Fig. 1 - (a) CAD model, (b) sample obtained by SLM.

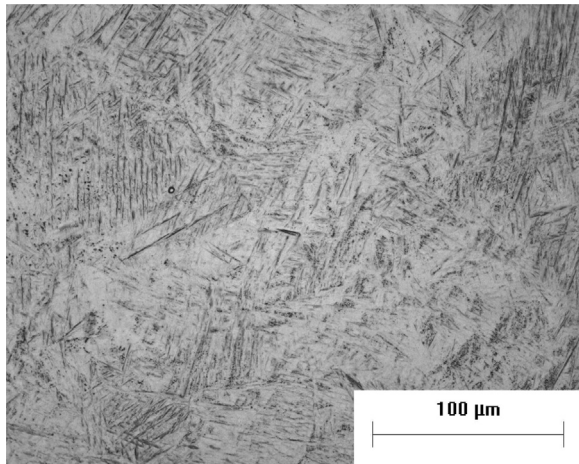


Fig. 2 – Martensitic α microstructure of the as-processed material.

A sample heat-treated at 1050 °C and slowly cooled inside the furnace was taken as a reference material. Such material is useful for purposes of comparison, since this treatment results in a coarse microstructure composed of α and β phases, which is a condition very close to thermodynamic equilibrium. Samples in this condition will be hereinafter referred to as a fully annealed sample. The as-processed samples as well as the fully annealed samples were characterized by differential scanning calorimetry (DSC), applying a heating rate of 10 K min⁻¹, and argon flow to prevent their oxidation. Another sample, heat-treated at 1050 °C and water quenched, was also used as a reference material because of its martensitic α microstructure, which was similar to that of the as-processed samples. The samples heat-treated at 1050 °C and water quenched are hereinafter referred to as water-quenched samples.

To prevent oxygen contamination during the heat treatment, the samples were encapsulated in quartz tubes under argon atmosphere. The parts were heated to the annealing temperature of 650 and 800 °C and annealed for 1 and 2 h, followed by cooling in air.

The heat-treated parts were also characterized by scanning electron microscopy (SEM) with energy dispersive X-ray spectroscopy (EDS) and X-ray diffraction (XRD). The samples were cut, embedded in resin, ground, polished and etched with Kroll's reagent in preparation for the SEM analysis.

Microhardness was measured using a Vickers indenter with a load of 2 N and a dwell time of 15 s, in accordance with the ASTM E384-11: Standard Test Method for Knoop and Vickers Hardness of Materials. The indentations were made on polished surfaces at the intersection of two struts, close to the center of the sample. The load of 2 N was chosen because it produces an indentation suitable for measuring the average hardness of the different phases in the heat-treated samples. Each value reported here represents the average of 15 tests. The E_{eff} , YS and UCS were determined based on compressive tests, in accordance with the ASTM E09-09: Standard Test Methods of Compression Testing of Metallic Materials at Room Temperature, using a universal testing machine equipped with a deflectionometer. The fracture strain, which quantifies the ductility of the material, was determined at the fracture point of the

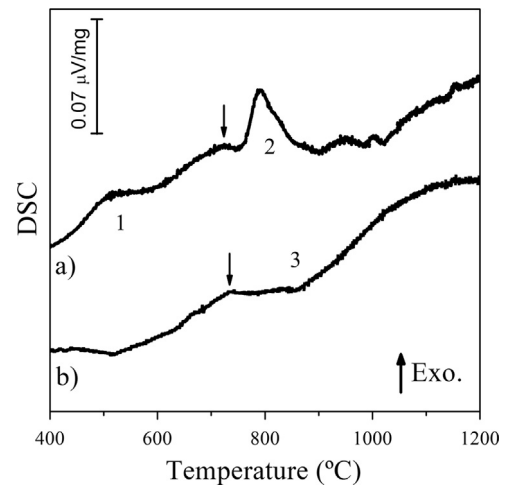


Fig. 3 – DSC thermograms of: (a) as-processed and (b) fully annealed samples.

compression curve. The tests were performed at room temperature, at a reduction rate of 2 mm/min. YS was determined at 0.2% offset. Each reported value represents the average of 3 tests.

3. Results

Fig. 3 shows the DSC thermograms of the as-processed and the fully annealed samples. The fully annealed sample presented a broader endothermic peak (indicated by 3) between approximately 735 and 1025 °C, which can be attributed to the $\alpha \rightarrow \beta$ transformation. It is known that Ti-6Al-4V is an $\alpha + \beta$ alloy and that the volumetric fraction of the α phase, which is about 90% at room temperature (Henry et al., 1995; Facchini et al., 2010), decreases with increasing temperature until it is completely transformed into β phase when the temperature reaches β -transus. According to the literature (Ahmed and Rack, 1998; Vrancken et al., 2012; Pederson et al., 2003; Fan et al., 2005; Veiga et al., 2012), the β -transus temperature of Ti-6Al-4V is about 970 ± 50 °C. Based on dilatometric experiments, Homporová et al. (2011) reported that the $\alpha \rightarrow \beta$ transformation in Ti-6Al-4V alloy with duplex microstructure occurs between 750 and 1050 °C. Hence, this result is in good agreement with the expected one, although it should be pointed out that the heating rate used in these DSC analyses led to superheating of the reaction, causing the β -transus to shift to higher values. The slow kinetics of the $\alpha \rightarrow \beta$ transformation at temperatures lower than 735 °C prevents its detection in DSC experiments.

The thermogram of the as-processed material shows two exothermic peaks, one occurring between 440 and 590 °C (indicated by 1) and the other between 760 and 850 °C (indicated by 2). The first exothermic peak may be ascribed to residual stress relaxation, since residual stress is reported in SLM parts (Shiomi et al., 2004; Mercelis and Kruth, 2006; Leuders et al., 2013). The second exothermic peak is presumably related with the decomposition of martensitic α' phase. This correlation can be made because the α' phase is metastable and should decompose in this temperature range, and this type of phase transformation produces an exothermic

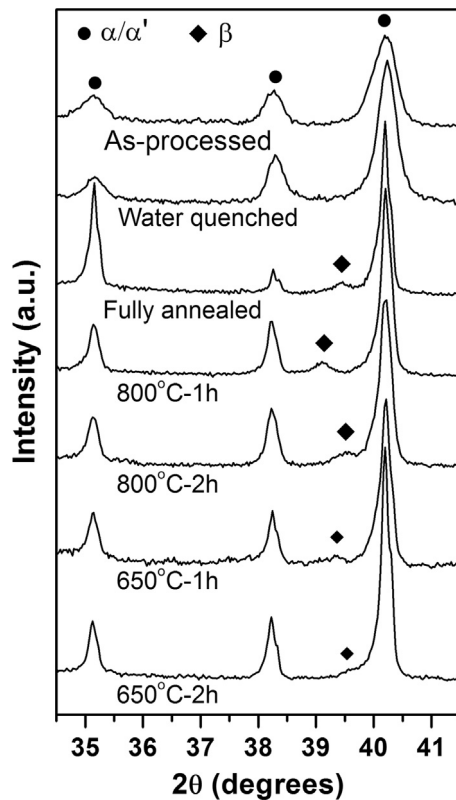


Fig. 4 – XRD patterns of SLM parts in the as-processed state and after different heat treatments.

peak. The absence of these exothermic peaks (1 and 2) in the thermogram of the fully annealed sample corroborates both associations. Also note the inflection point (indicated by an arrow) at 715 °C, which occurs at a slightly lower temperature than that of the onset of the second exothermic peak. This inflection point seems to represent the onset of an endothermic peak, which was overlapped by the exothermic peak. This inflection point appears at a temperature very close to that of the onset of the endothermic peak (also indicated by an arrow) of the $\alpha \rightarrow \beta$ transformation in the thermogram of the fully annealed sample, suggesting that the inflection point may indicate the onset temperature of an endothermic peak pertaining to a reaction similar to that of the $\alpha \rightarrow \beta$ transformation, which occurred in the fully annealed sample.

Fig. 4 shows the XRD patterns of the SLM parts in the as-processed state and after different heat treatments. For purposes of comparison, we have included the thermograms of the fully annealed sample and of the sample heat-treated at 1050 °C and water quenched, whose microstructure (α') is similar to that of the as-processed samples.

The as-processed sample and the one heat-treated at 1050 °C and water quenched present only peaks related the hexagonal close-packed crystalline structure of titanium (hcp-Ti). These peaks are indicated by α/α' , since both α and α' phases have the hexagonal compact structure and produce XRD peaks in similar angular positions. The metallurgical difference between α and α' is basically the amount of solute element in the atomic structure. Diffusion of the solute during fast cooling is prevented; hence, the martensitic α'

Table 1 – FWHM of the main α/α' peak at $2\theta \approx 40.2$ of samples subjected to different heat treatments.

Material	FWHM
As-processed condition	0.45
Water-quenched condition	0.33
Fully annealed condition	0.19
Heat-treated at 800 °C for 1 h	0.20
Heat-treated at 800 °C for 2 h	0.16
Heat-treated at 650 °C for 1 h	0.17
Heat-treated at 650 °C for 2 h	0.20

phase has a higher vanadium content than the equilibrium α phase. A higher solute content promotes greater deformation of the crystal structure, which broadens the XRD peaks. On the other hand, the fully annealed sample presents XRD peaks corresponding to both α/α' and β phases. The intensity of the XRD peak of the β phase is weak due to the low volume fraction of β phase in the alloy at room temperature. The main peak of the α/α' phase ($2\theta \approx 40.2$) was adjusted using two Lorentzian functions, and its full width at half maximum (FWHM) corresponding to Cu-K α_1 radiation was measured. Table 1 presents the results. As can be seen, the FWHM values of the as-processed sample and the one heat-treated at 1050 °C and water quenched are significantly higher than those of the other samples, because these samples are composed of martensitic α' phase.

The samples heat-treated at 800 °C also show XRD peaks corresponding to both α/α' and β phases. However, the XRD peak of β phase observed in the sample heat-treated for 1 h is shifted to a lower angular position. The samples heat-treated at 650 °C at both annealing times clearly show only XRD peaks corresponding to the α/α' phase, while the peak corresponding to the β phase may be present, as indicated in the XRD patterns, but at the limit of detection. Moreover, the shift to a lower angular position of the XRD peak of the β phase in the sample heat-treated at the lower temperature for 1 h seems to have occurred in the same way as in the sample heat-treated at 800 °C for 1 h.

The microstructures of the samples heat-treated at 650 and 800 °C for 1 or 2 h were analyzed by SEM and are depicted in Fig. 5 under low and high magnification. Under lower magnification (Fig. 5a and c), the microstructure of the samples heat-treated at 650 °C for 1 or 2 h appears to be α' , since its typical fine needles are clearly visible. Using SEM in backscattered electron mode, the presence of β phase is detectable by chemical contrast, appearing with a brighter aspect, since vanadium has a higher atomic mass than titanium and the β phase has a higher vanadium content than the α phase. So, when observed under higher magnification, the β phase is clearly visible in the sample treated for 2 h (Fig. 5d), in the form of flat particles located along the α' needle boundaries. The β phase was not observed in the sample treated at 650 °C for 1 h (Fig. 5b).

In the case of the samples heat-treated at 800 °C, the low magnification image shows a fine $\alpha+\beta$ microstructure (Fig. 5e and g). Under high magnification (Fig. 5f and h), note that the

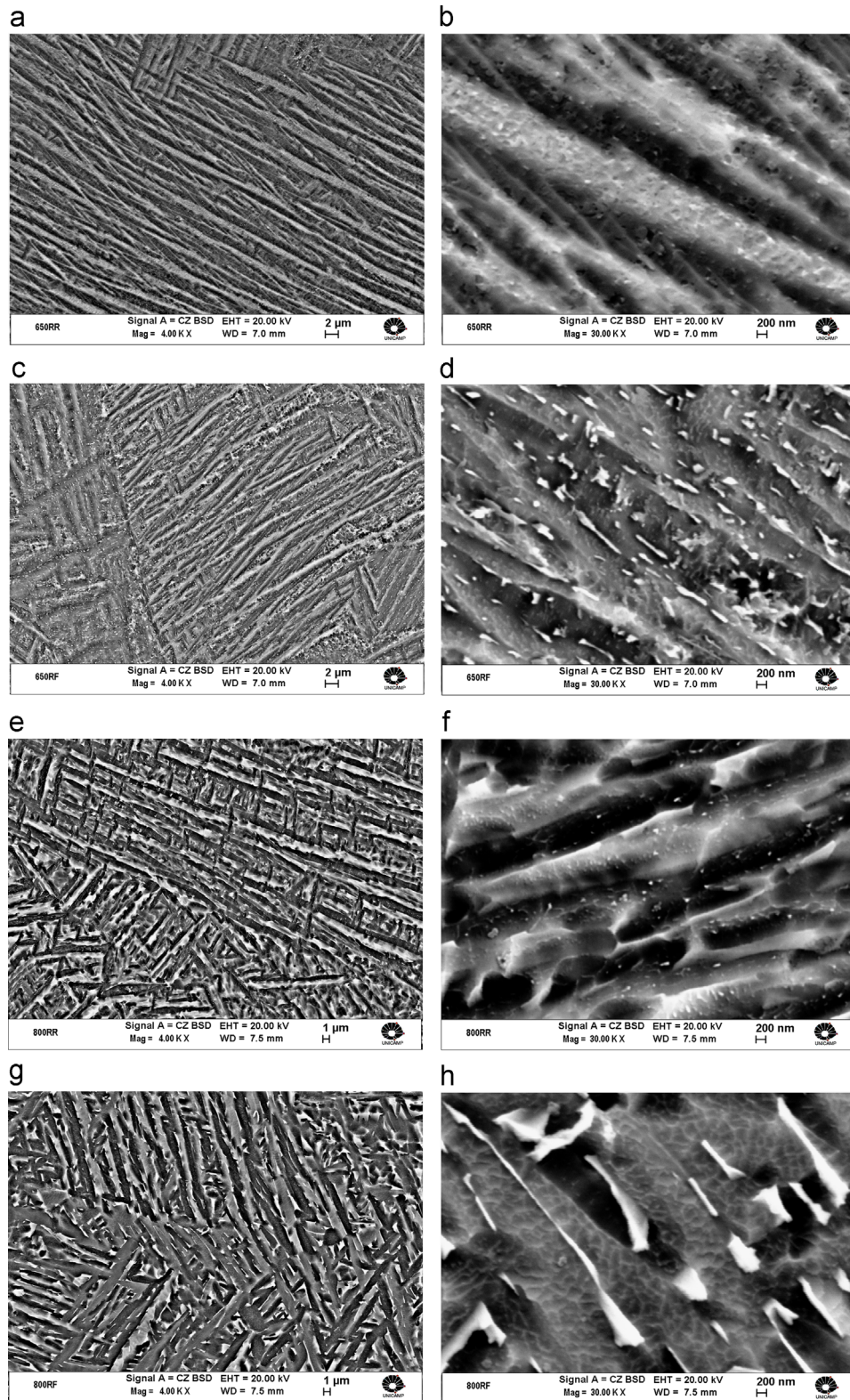


Fig. 5 – SEM micrographs of samples heat-treated at 650 °C for 1 h (a and b) and for 2 h (c and d), at 800 °C for 1 h (e and f) and for 2 h (g and h).

particles of β phase are located along the boundaries of the original α' needles, presenting an aspect similar to that observed in the samples treated at 650 °C for 2 h. However, the particles are fewer in number and larger in size.

An EDS analysis was performed to confirm the concentration of vanadium in the brighter particles identified as β phase precipitation. However, some limitations inherent to this technique must be taken into account. The interaction

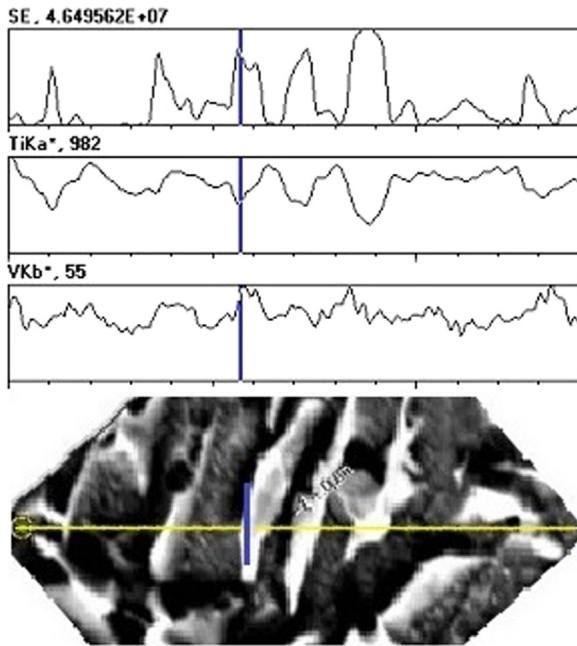


Fig. 6 – EDS analysis in line scan and the respective secondary electron (SE), Ti- K_{α} and V- K_{β} lines, of the sample heat-treated at 800 °C for 2 h.

volume between the incident electrons and the material, using 10 kV, has a diameter of about 300 nm, which is more than twice the average thickness of the β phase particles after heat treatment at 800 °C for 2 h (see Fig. 5g). Moreover, the energy of vanadium K_{α} is coincident with that of titanium K_{β} . Hence, vanadium K_{β} must be used to estimate the vanadium content. In this context, the quantitative results of vanadium content in these thinner particles are inaccurate. Therefore, a semi-quantitative EDS analysis in line scan over a small region across some brighter particles (see Fig. 6) was performed to confirm the higher vanadium content of these particles. The sample heat-treated at 800 °C for 2 h was used for this purpose, since its brighter particles are larger than those of the samples subjected to other sub- β -transus heat treatments. The secondary electron line (SE), which reveals the topography of the scanned line, shows that the brighter particles are protuberances on the surface. The Ti- K_{α} and V- K_{β} lines indicated a decrease in titanium and a corresponding increase in vanadium. Hence, this analysis suggests that the greater brightness of the particles is due partly to the border effect of the protuberances and partly to the higher content of vanadium, which was used to recognize the particles as corresponding to β phase precipitation.

As postulated, SLM Ti-6Al-4V parts present acicular α martensitic microstructure, which ductility is low, hence heat treatments can be useful to overcome this disadvantage. Fig. 7 shows the compression curves of samples in three different conditions: as-processed, fully annealed, and heat-treated at 800 °C for 2 h. The low ductility of the as-processed condition was confirmed, as expected. The higher fracture strain and the lower strength of the sample in the fully annealed condition are also shown. These results indicate that the fracture strain was increased with a minor decrease

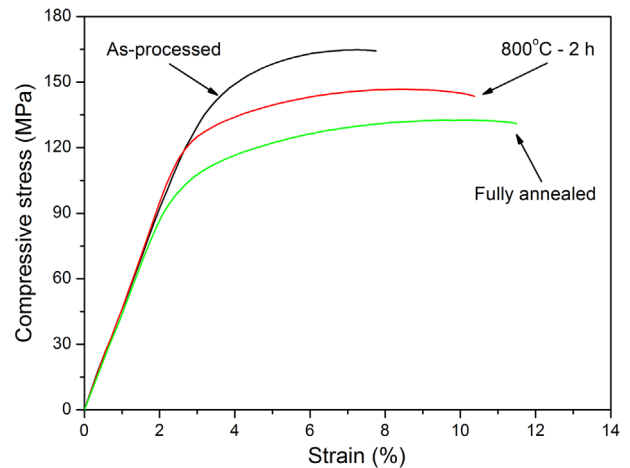


Fig. 7 – Compression curves of samples in three different conditions: as-processed, fully annealed, and heat-treated at 800 °C for 2 h.

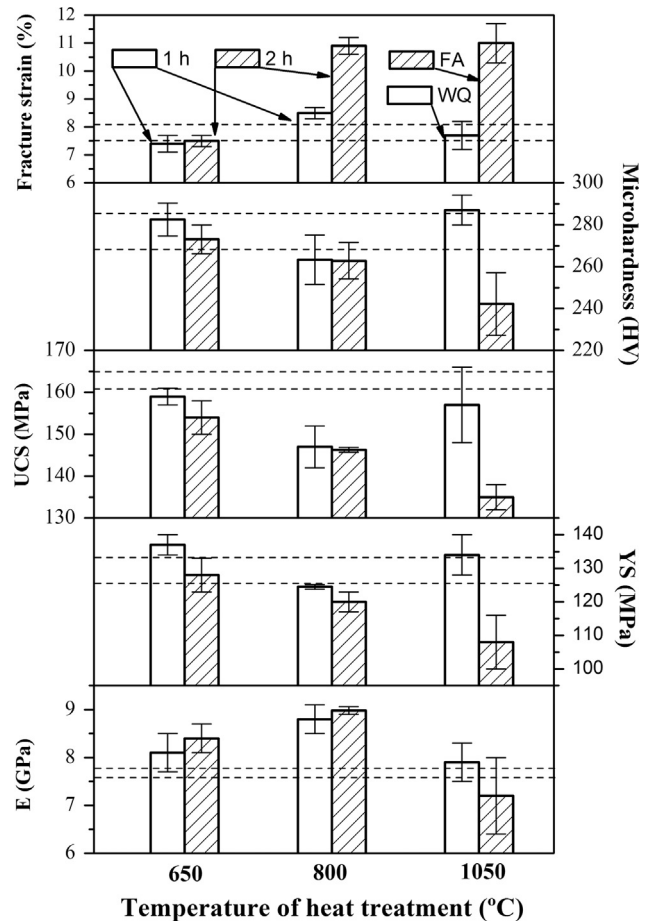


Fig. 8 – Young's modulus, yield and ultimate compressive strength, fracture strain and microhardness of the porous parts fabricated by SLM, heat-treated at 650 and 800 °C for 1 and 2 h, at 1050 °C and water quenched (WQ) or furnace cooled (fully annealed, FA). The dashed lines show the mean plus standard deviation and the mean minus standard deviation of each property of the porous parts in the as-processed state.

in UCS when the heat treatment at 800 °C for 2 h was applied. These curves also allowed for the determination of the E_{ff} of the samples in these conditions. Despite the very similar values, note that the E_{ff} of the fully annealed sample is lower than that of the sample heat-treated at 800 °C for 2 h. Fig. 8 summarizes all the results of the microhardness and compressive tests. The values obtained from the compression curves are the mean of 3 tests, plus the standard deviation. The microhardness results represent the average of 15 tests. The dashed lines indicate the mean plus standard deviation and the mean minus standard deviation of each property of the porous parts in the as-processed state.

The properties of the samples water quenched from 1050 °C and of the fully annealed samples were plotted for purposes of comparison. The water-quenched samples showed properties statistically similar to those of the as-processed samples, as both conditions present the martensitic α' microstructure. In contrast, the fully annealed samples showed a decrease in E_{ff} , hardness, YS and UCS and an increase in ductility (fracture strain). This performance can be attributed to the coarse $\alpha+\beta$ microstructure that developed during cooling in the furnace.

Considering only the samples subjected to treatments at sub- β -*transus* temperatures, the results of hardness, YS, UCS and fracture strain were found to be dependent on time and temperature. As a general rule, in response to increasing treatment time or temperature, hardness, YS and UCS decreased while fracture strain increased. The results of UCS and hardness of the samples heat-treated at 800 °C for both annealing times were statistically similar. Moreover, considering only the samples subjected to treatments at sub- β -*transus* temperatures, the values of E_{ff} were also time- and temperature-dependent: higher temperatures or longer treatment times resulted in stiffer samples, although the effect of treatment time was statistically less significant than that of temperature.

4. Discussion

Knowledge about the microstructure of as-processed materials and their thermal behavior is an important step in designing heat treatments for parts produced by SLM. As comprehensively shown (Sallica-Leva et al., 2013), Ti-6Al-4V parts produced by SLM present the α' microstructure. As stated earlier herein, the α' phase has the same crystal structure as the α phase, but its vanadium content is higher. In fact, the α' phase is supersaturated in vanadium. The greater distortion of the α' crystal structure due to the martensitic transformation and the consequent supersaturation of alloying elements, which caused broadening of the α/α' XRD peaks (see Fig. 4 and Table 1), promotes a hardening effect, but this effect is only moderate in Ti-6Al-4V alloy (Leyens and Peters, 2003). As a supersaturated solid solution, α' is a metastable phase and the degree of its transformation into phases closer to or in thermodynamic equilibrium during sub- β -*transus* heat treatment will determine the features of the heat-treated samples.

The analysis of the SEM microstructures shows that the β phase nucleated along the boundary of the α' needles. Since α' is supersaturated in vanadium and the β phase is able to

solubilize a significantly greater amount of vanadium than the α phase, vanadium begins to diffuse from α' to β phase after β phase nucleation. This diffusion decreases the vanadium content in α' ; hence, α' gradually converges toward α phase. This explanation is in accordance with the results reported by Chao et al. (2014), who proposed a grain refinement method by thermomechanical processing of a martensitic α' microstructure of Ti-6Al-4V. These authors also described β phase nucleation along the boundary of α' needles. However, this explanation contradicts what Vrancken et al. (2012) postulated. The latter authors, who also analyzed heat treatments in SLM parts, stated that α is the phase that nucleates along the boundary of α' needles when heated, rejecting vanadium atoms and leading to the formation of β phase at the α phase boundaries; however, they did not offer evidence of α being nucleated in α' .

The thermal analysis can provide additional support to this question. As indicated by the thermograms in Fig. 3, the onset temperature of the exothermic peak corresponding to martensite α' decomposition is slightly higher than that of the endothermic peak of the $\alpha\rightarrow\beta$ phase transformation that occurred in the fully annealed samples. Also, the thermogram of the as-processed sample seems to present an endothermic peak pertaining to a reaction similar to the $\alpha\rightarrow\beta$ transformation, which was overlapped by the exothermic peak of martensite α' decomposition. The onset of this peak occurred at a temperature about 45 °C lower than the onset temperature (760 °C) of the exothermic peak of martensite α' decomposition. The analysis of microstructures shown in Fig. 5 suggests that this endothermic peak was produced by the precipitation of β phase, since particles of β phase are visible along the boundary of the α' needles in the samples heat-treated at 650 °C for 2 h and at 800 °C for both the annealing times. The precipitation of β phase (or $\alpha'\rightarrow\beta$ transformation) enabled the vanadium to diffuse from the remaining α' to β phase, decreasing the supersaturation of α' and producing the exothermic peak attributed to martensite decomposition. Hence, the precipitation of β is necessary to accommodate the excess of vanadium that will be rejected from the α' , and we can argue that the decomposition of martensite occurs as follows: precipitation of β phase along the boundary of α' needles and diffusion of vanadium from α' to β phase, decreasing the free energy stored as supersaturation of a solid solution and gradually transforming α' into α phase.

The $\alpha\rightarrow\beta$ (in the fully annealed sample upon heating) and $\alpha'\rightarrow\beta$ (precipitation of β phase in the as-processed sample upon heating) transformations were detected at very similar temperatures in the thermal analysis, although the $\alpha'\rightarrow\beta$ transformation was overlapped by the martensite decomposition. However, it should be noted that the $\alpha\rightarrow\beta$ transformation that occurred in the fully annealed sample did not require the nucleation of β particles, since this phase was already present in the starting microstructure. In this case, there was only β phase growth. On the other hand, in the as-processed sample, the β phase precipitation required a nucleation process. Another consideration is the greater distance of the martensitic microstructure from equilibrium at temperatures above 700 °C, in which both the $\alpha\rightarrow\beta$ and the $\alpha'\rightarrow\beta$ transformations were detected in the thermal analysis.

A comparison of the XRD patterns of the as-processed sample and the one heat-treated at 800 °C for 1 h reveals two

main differences: the appearance of the peak corresponding to the β phase and the decrease in the FWHM of the α/α' main peak. The presence of the peak corresponding to the β phase corroborates the precipitation of β phase observed by SEM, while the vanadium diffusion out of the α' , which reduced the supersaturation and, as a consequence, the deformation of the crystal structure, is corroborated by the decrease in the FWHM of the α/α' main peak.

The main difference that can be detected when comparing the XRD patterns of the samples heat-treated at 800 °C for 1 and 2 h is the shift of the peak corresponding to the β phase to a higher angle resulting from the longer treatment time. The 2θ angle related with the (110) peak of the β titanium phase shifted from 39.43 (800 °C – 1 h) to 39.89 (800 °C – 2 h). The lattice parameter of β phase was calculated based on Bragg's law (Cullity, 1978), considering Cu- $K_{\alpha 1}$ radiation. The (110) planar distances were found to be equal to 22.83 nm (800 °C – 1 h) and 22.58 nm (800 °C – 2 h) and the lattice parameters equal to 32.29 nm (800 °C – 1 h) and 31.93 nm (800 °C – 2 h). The lower lattice parameter of the sample heat-treated for 2 h indicates that a higher vanadium content was dissolved in the titanium β phase, since vanadium has a lower atomic radius than titanium (the atomic radiuses of titanium and vanadium are 0.146 and 0.132 nm, respectively (Calin et al., 2013)). Hence, the XRD results indicate that the vanadium content in the β phase increased as a function of treatment time. The relationship between vanadium content and time indicates that β phase enrichment in vanadium is controlled by diffusion, which means that the martensite decomposition process is dependent on soak time and temperature.

Based on their analysis of the kinetics of martensite decomposition in Ti-6Al-4V alloys with additions of hydrogen, Qazi et al. (2003) stated that martensite decomposition upon heating is, in fact, a soak time- and temperature-dependent process and that there is an incubation time during which martensite does not decompose. Hence, the time-temperature-transformation (TTT) diagram can be determined, and is naturally nose-shaped. These authors also stated that the temperature at which martensite in Ti-6Al-4V alloys is less stable (the nose temperature) is about 800 °C. This statement can explain the longer time required to produce detectable β phase precipitation at 650 °C. One hour at 650 °C did not produce β phase precipitation detectable by SEM (Fig. 5b), but 1 h at 800 °C sufficed to produce it (Fig. 5f).

The degree of martensite decomposition will determine the balance between mechanical strength and ductility in sub- β -transus heat treatments, such as in the tempering of martensite in steels, albeit of lower intensity. Due to the very fine acicular morphology and hardening of the solid solution, the martensitic α' microstructure presents higher strength than the same alloy with $\alpha+\beta$ microstructure (Matsumoto et al., 2011). In addition to eliminating residual stress, heat treatments of SLM parts can be used to increase ductility, albeit with some loss in strength.

In incomplete martensite decomposition, the volume fraction and the vanadium content of β phase did not reach the equilibrium condition, i.e., both of them were lower than the values of the equilibrium condition. Consequently, the volume fraction and vanadium content of the α/α' phase were higher than those of the equilibrium condition.

The degree of α/α' phase supersaturation, which is a consequence of the degree of martensite decomposition,

appeared to exert the most significant influence on the hardness, strength and fracture strain of the heat-treated parts in this work. The SEM analysis indicated that martensite decomposition did not begin during the heat treatment at 650 °C for 1 h. Therefore, the properties of the samples heat-treated at 650 °C for 1 h were statistically similar to those of the as-processed samples. After 2 h at the same temperature, a minor degree of martensite decomposition occurred, as shown in the microstructure in Fig. 5d. Thus, hardness and strength tend to decrease and fracture strain to increase in response to increasing annealing time. In the case of samples heat-treated at 800 °C, the decrease in strength and increase in ductility (fracture strain) of the heat-treated parts were unequivocal. In this case, the martensite did not decompose completely in the first hour of annealing, as indicated by the lower vanadium content of the β phase (lower angle of diffraction of the XRD peak). However, 2 h at 800 °C seems to have produced complete martensite decomposition, as indicated by the XRD pattern (upward shift of the β phase peak) and by the thermal analysis (the temperature of the exothermic peak indicated by 3). In addition to complete martensite decomposition, sub- β -transus treatments are known to prevent grain growth, because β and α prevent each other's growth (Vrancken et al., 2012). The consequence of complete martensite decomposition, allied to a refined microstructure, was that the fracture strain approximated that of the fully annealed samples, whereas the hardness and strength was similar to those of the samples heat-treated at the same temperature for 1 h, and significantly greater than those of the fully annealed samples. Hence, the use of heat treatments to promote martensite decomposition while maintaining the refined microstructure is a suitable alternative to improve the mechanical properties of SLM parts. Vrancken and co-authors reported similar results, i.e., increasing fracture strain and decreasing YS in response to increasing annealing temperature in the sub- β -transus region.

It is known that the $\alpha+\beta$ phases are the final products of martensite α' decomposition in Ti-6Al-4V alloy. As shown here, this transformation is the sum of two almost simultaneous transformations: the precipitation of β phase ($\alpha'\rightarrow\beta$) and the loss of excess vanadium in the α' solid solution, which gradually transforms α' into α phase ($\alpha'\rightarrow\alpha$).

The different phases in titanium alloys present different Young's moduli. A basic sequence of decreasing Young's modulus is $\alpha>\alpha'>\beta$ (Crespo, 2011). Hence, the $\alpha'\rightarrow\alpha+\beta$ transformation simultaneously produces a phase with lower stiffness ($\alpha'\rightarrow\beta$) and a phase with higher stiffness ($\alpha'\rightarrow\alpha$). The increase in the E_{ff} of the parts heat-treated at 650 °C or 800 °C indicates that the effect of $\alpha'\rightarrow\alpha$ transformation prevailed over that of the $\alpha'\rightarrow\beta$ transformation. On the other hand, the lower E_{ff} of the fully annealed samples when compared to that of the samples with martensitic α' microstructure (the as-processed and the quenched samples) demonstrates that the transformation that prevailed was $\alpha'\rightarrow\beta$.

5. Conclusions

In this study, we examined the effects of sub- β -transus heat treatments on the mechanical properties of Ti-6Al-4V porous

structures produced by SLM, emphasizing the role of martensite α' phase decomposition.

It was proposed that the decomposition of martensite started with the precipitation of β phase at the boundaries of α' needles. This phase nucleation enabled the vanadium to diffuse from α' to β phase, decreasing the free energy stored as supersaturation of a solid solution and gradually transforming α' into α phase. The precipitation of β phase produced an endothermic peak with an onset temperature of 715 °C in the thermogram of the as-processed sample. The decrease in the supersaturation of α' produced an exothermic peak between 760 and 850 °C.

The XRD patterns of the samples heat-treated at 800 °C presented clearly visible peaks corresponding to α/α' and β phases, which resembled those in the thermogram of the fully annealed sample. The samples heat-treated at 650 °C presented XRD peaks corresponding to α/α' and the main β phase peak was located at the limit of detection. The as-processed sample presented only peaks pertaining the α/α' crystalline structure of titanium.

The SEM analyses revealed that the microstructure of samples heat-treated at 650 °C for 1 h was very similar to that of the starting condition, with fine α' needles. On the other hand, the samples heat-treated at 650 °C for 2 h and at 800 °C for 1 and 2 h showed microstructures still containing the fine α' needles of the starting condition, with flat particles of β phase located along the α' needle boundaries.

The degree of martensite decomposition during the sub- β -*transus* heat treatment determined the changes identified in the alloy's mechanical properties, i.e., hardness, YS and UCS decreased while fracture strain increased.

The samples heat-treated at 800 °C for 2 h underwent complete martensite decomposition while maintaining their refined microstructure, which increased the ductility (fracture strain) to values approximating that of the fully annealed samples, with a minor decrease in hardness and strength.

The martensite decomposition increased the E_{ff} of the samples subjected to sub- β -*transus* heat treatment owing to the transformation of α' into α phase.

Acknowledgments

The authors would like to thank the São Paulo State Research Foundation (FAPESP, Brazil) (Grant 2011/19982-2), and the National Council for Scientific and Technological Development (CNPq, Brazil) (Grant 483733/2010-5) for their financial support, and the Brazilian Federal Agency for Support and Improvement of Higher Education (CAPES, Brazil) for the scholarship granted to the first author, and Professor Alberto Moreira Jorge Junior, of the Structure Characterization Laboratory (LCE, Federal University of São Carlos, Brazil).

REFERENCES

Ahmed, T., Rack, H.J., 1998. Phase transformations during cooling in alpha+beta titanium alloys. *Mater. Sci. Eng. A* 243, 206–211.
 Calin, M., Gebert, A., Ghinea, A.C., Gostin, P.F., Abdi, S., Mickel, C., Eckert, J., 2013. Designing biocompatible Ti-based metallic

glasses for implant applications. *Mater. Sci. Eng. C* 33 (2), 875–883.
 Chao, Q., Hodgson, P.D., Beladi, H., 2014. Ultrafine grain formation in a Ti–6Al–4V alloy by thermomechanical processing of a martensitic microstructure. *Metall. Mater. Trans. A* 45, 2659–2671.
 Crespo, A., Amimul Ahsan, 2011. Modelling of heat transfer and phase transformations in the rapid manufacturing of titanium components. In: Ahsan, A. (Ed.), *Convection and Conduction Heat Transfer*. Intech, pp. 315–340 (ISBN 978-953-307-582-2).
 Cullity, B.D., 1978. *Elements of X-ray Diffraction*, second ed. Addison-Wesley, United State of America.
 Dong, J., Li, F., Wang, C., 2013. Micromechanical behavior study of α phase with different morphologies of Ti–6Al–4V alloy by microindentation. *Mater. Sci. Eng. A* 580, 105–113.
 Elmer, J.W., Palmer, T.A., Babu, S.S., Zhang, W., DebRoy, T., 2004. Phase transformation dynamics during welding of Ti–6Al–4V. *J. Appl. Phys.* 95, 8327–8339.
 Facchini, L., Magalini, E., Robotti, P., Molinari, A., Höges, S., Wissenbach, K., 2010. Ductility of a Ti–6Al–4V alloy produced by selective laser melting of prealloyed powders. *Rapid Prototyp. J.* 16, 450–459.
 Fan, Y., Cheng, P., Yao, Y.L., Yang, Z., Eglund, K., 2005. Effect of phase transformations on laser forming of Ti–6Al–4V alloy. *J. Appl. Phys.* 98, 013518.
 Fan, Y., Shipway, P.H., Tansley, G.D., Xu, J., 2011. The effect of heat treatment on mechanical properties of pulsed Nd: YAG welded thin Ti6Al4V. *Adv. Mater. Res.* 189–193, 3672–3677.
 Geetha, M., Singh, A.K., Asokamani, R., Gogia, A.K., 2009. Ti based biomaterials, the ultimate choice for orthopaedic implants – a review. *Prog. Mater. Sci.* 54, 397–425.
 Henry, S.D., Davidson, G.M., Lampman, S.R., Reidenbach, F., Boring, R.L., Scott Jr, W.W., 1995. *Fatigue Data Book: Light Structural Alloy*, ASM Handbook. ASM International, USA.
 Homporová, P., Poletti, C., Stockinger, M., Warchomicka, F., 2011. Dynamic phase evolution in titanium alloy Ti–6Al–4V. In: Zhou, L. (Ed.) *Proceedings of the 12th World Conference on Titanium*. Beijing, China, pp. 19–42.
 Leuders, S., Thöne, M., Riemer, A., Niendorf, T., Tröster, T., Richard, H.A., Maier, H.J., 2013. On the mechanical behaviour of titanium alloy TiAl6V4 manufactured by selective laser melting: fatigue resistance and crack growth performance. *Int. J. Fatigue* 48, 300–307.
 Leyens, C., Peters, M., 2003. *Titanium and Titanium Alloys: Fundamentals and Applications*. Wiley-VCH Verlag GmbH & Co. KGaA, Weinheim, Germany.
 Liu, X., Chu, P.K., Ding, C., 2004. Surface modification of titanium, titanium alloys, and related materials for biomedical applications. *Mater. Sci. Eng. R* 47, 49–121.
 Lütjering, G., 1998. Influence of processing on microstructure and mechanical properties of (α + β) titanium alloys. *Mater. Sci. Eng. A* 243, 32–45.
 Matsumoto, H., Yoneda, H., Sato, K., Kurosu, S., Maire, E., Fabregue, D., Konno, T.J., Chiba, A., 2011. Room-temperature ductility of Ti–6Al–4V alloy with α' martensite microstructure. *Mater. Sci. Eng. A* 528, 1512–1520.
 Mercelis, P., Kruth, J.P., 2006. Residual stresses in selective laser sintering and selective laser melting. *Rapid Prototyp. J.* 12, 254–265.
 Murr, L.E., Quinones, S.A., Gaytan, S.M., Lopes, M.I., Rodela, A., Martinez, E.Y., Hernandez, D.H., Martinez, E., Medina, F., Wicker, R.B., 2009. Microstructure and mechanical behavior of Ti–6Al–4V produced by rapid-layer manufacturing, for biomedical applications. *J. Mech. Behav. Biomed. Mater.* 2, 20–32.
 Parthasarathy, J., Starly, B., Raman, S., Christensen, A., 2010. Mechanical evaluation of porous titanium (Ti6Al4V) structures with electron beam melting (EBM). *J. Mech. Behav. Biomed. Mater.* 3, 249–259.

- Pederson, R., Babushkin, O., Skystedt, F., Warren, R., 2003. Use of high temperature X-ray diffractometry to study phase transitions and thermal expansion properties in Ti-6Al-4V. *Mater. Sci. Technol.* 19, 1533–1538.
- Qazi, J.I., Senkov, O.N., Rahim, J., Froes, F.H., 2003. Kinetics of martensite decomposition in Ti-6Al-4V-xH alloys. *Mater. Sci. Eng. A* 359, 137–149.
- Sallica-Leva, E., Jardini, A.L., Fogagnolo, J.B., 2013. Microstructure and mechanical behavior of porous Ti-6Al-4V parts obtained by selective laser melting. *J. Mech. Behav. Biomed. Mater.* 26, 98–108.
- Shiomi, M., Osakada, K., Nakamura, K., Yamashita, T., Abe, F., 2004. Residual stress within metallic model made by selective laser melting process. *CIRP Ann. Manuf. Technol.* 53, 195–198.
- Vandenbroucke, B., Kruth, J.P., 2007. Selective laser melting of biocompatible metals for rapid manufacturing of medical parts. *Rapid Prototyp. J.* 13, 196–203.
- Veiga, C., Davim, J.P., Loureiro, A.J.R., 2012. Properties and applications of titanium alloys: a brief review. *Rev. Adv. Mater. Sci.* 32, 133–148.
- Venkatesh, B.D., Chen, D.L., Bhole, S.D., 2009. Effect of heat treatment on mechanical properties of Ti-6Al-4V ELI alloy. *Mater. Sci. Eng. A* 506, 117–124.
- Vrancken, B., Thijs, L., Kruth, J.P., Van Humbeeck, J., 2012. Heat treatment of Ti6Al4V produced by selective laser melting: microstructure and mechanical properties. *J. Alloy. Compd.* 541, 177–185.
- Warnke, P.H., Douglas, T., Wollny, P., Sherry, E., Steiner, M., Galonska, S., Becker, S.T., Springer, I.N., Wiltschko, J., Sivanathan, S., 2009. Rapid prototyping: porous titanium alloy scaffolds produced by selective laser melting for bone tissue engineering. *Tissue Eng. C – Methods* 15, 115–124.
- Yang, S., Leong, K.F., Du, Z., Chua, C.K., 2002. The design of scaffolds for use in tissue engineering. Part II. Rapid prototyping techniques. *Tissue Eng.* 8, 1–11.